THE CYCLIC YIELD RESPONSE OF A STEEL STAR PLATE CRUCIFORM JOINT

R. N. Croad*, F. H. Mead**, R. Shepherd***

ABSTRACT

This paper is a summary of an investigation into the cyclic response of a steel cruciform joint. A star plate beam to column joint identical to one of those forming the frame of the pier structure at Auckland International Airport was tested at the University of Auckland, School of Engineering. In this paper both the preparations undertaken and the subsequent experimental programme are described. The results are analysed and the observed behaviour is discussed. Comparisons are made with recently proposed design criteria for steel beam to column connections, as well as with formulae for predicting the load-deflection curves. Conclusions are drawn on the suitability of these theories for response prediction of star plate geometry joints. Additionally the energy absorption capabilities of the joint are compared with results from earlier American research.

1.1 THE TEST SPECIMEN

The star plate joint which was tested is shown three-dimensionally in Fig. 1. The joint comprised two ⅜" thick star plates connected by a stub box column cut as a short length from the normal 14" square box column members. Box column sections were welded on to the upper and lower faces of the star plate joint. Half inch plates for beam web connections were welded between the star plates and to the stub boxes. The star plates act in three ways:

(a) to transfer beam flange forces across the joint in the plane of the plate,

(b) to transfer column forces across the joint in through thickness direction of the plate, i.e. normal to the plane of the plate, and

(c) to act as diaphragn stiffeners to the joint.

As it was normal practice during fabrication to drill two holes at the centre of the star plates to assist in aligning up the joint before welding, these holes were suitably enlarged to allow a prestressing Macalloy bar to pass through the length of the column and thus provide axial load for the purposes of the test.

Stub beams were welded onto the projecting wings of the star plates, the lower wing being wider than the upper in order to facilitate down hand welding on site where the connection is normally made. The ends of the beams were provided with pressure pads and holding recesses for the loading rams. Star plates with three 'wings' only were used to enable the test specimen to fit into the reaction frame, and two beams only were provided to suit the single plane joint loading that could be accommodated in the available test rig.

The column ends had 15" square x 2" thick capping plates, plus 11" square x 1½" thick plate bearing pads for the stressing nuts of the 40mm dia. Macalloy prestressing rod.

This type of joint was selected for the pier structure based on experience gained on a previous project where a similar steel frame joint had been used with success.

All plate, including that used for the box columns conformed with B.S.4360 grade 43C (notch ductile). Box columns were fabricated using an automatic submerged arc process from ¾" plate using partial penetration V groove welds.

Star plate material was examined before profile marking for lamination or high inclusion clusters using an ultrasonic probe operating on a general grid pattern. After marking out the areas of plate abutting the columns where butt welds would be made and where the plates would be subjected to through thickness stresses in addition to normal planar stresses, these critical regions were more closely and continuously inspected before cutting using the same ultrasonic technique. Details of the butt weld are shown in Fig. 2.

The joint was preheated and manually welded in rotators using low hydrogen electrodes. The welds were laid in a defined sequence and interpass temperatures maintained throughout the welding operation. After welding the joint was carefully examined for defects and for laminations in the star plates using double angled ultrasonic probes. On the project four joints were found after fabrication to have

* Research Student, Department of Civil Engineering, University of Auckland.
** District Materials and Investigating Engineer, New Zealand Ministry of Works and Development, Auckland.
*** Associate Professor of Civil Engineering, University of Auckland.

laminations out of a total of 392 joints completed. These were repaired by arc air gouging and rewelding followed by a further ultrasonic inspection.

It should be noted that the opportunity to test this joint came about due to the unexpected availability of a test rig recently constructed for use on another project. A limited time was offered between tests for that project, and so that the opportunity was not lost, a joint was taken from the fabrication production line. The only joint available at the time was one which had been repaired for lamellar tearing. In this respect therefore the joint is untypical of the joints in the structure in that it was one of the four which had received lamellar tear repairs.

Equally important to bear in mind is that the test was carried out as a practical investigation into joint behaviour and not as fundamental research. Had there been more time to consider test arrangements a more comprehensive test programme could have been pursued.

Before fabrication of joints for the structure was commenced, weld procedure tests were executed on a full size specimen joint so as to repeat exactly the highly restrained conditions in the work. Specimens were cut from that joint for examination and physical testing. The specimens successfully passed all tests.

Important aspects of the butt weld joint design - the geometry of which was governed by the need to keep weld metal deposits to a minimum and yet allow ample access for the adoption of sound welding techniques - were to limit through thickness stresses in the star plates under load and to reduce the possibility of failure initiation by stress concentrations at notches. The former was overcome by limiting the stress through the plate in a direction normal to its plane to approximately 50% its yield stress when the column plate was yielding in tension. This was achieved by stress dispersion through reinforcement at both the weld face and into the backing strip. The arrangement was checked by tension tests in which all specimens failed due to yielding in the column plate and not due to rupture of the star plate. Notch problems were checked by photo-elastic model tests in which the effect of profile 'notches' were examined and fears concerning crack initiation at the weld root were dispelled.

1.2 LOADING REGIME

The design for the Auckland Airport International Terminal structure commenced in late 1969. A typical section through the building frame for the aircraft loading pier is indicated schematically in Fig. 3. In this section the length of each bay is 33'4" and the column heights are 14'7½" for the ground floor, and 15' for the first floor. Frames are spaced at 20' centres. The orientation of the joint in the frame is indicated by the encircled diagram.

Deformation of the frame has been indicated corresponding to a horizontal ground movement. In this deformed state simultaneous vertical ground acceleration induces an axial load in the column, in addition to gravity loads and those induced by overturning forces, acting so as to cause an additional eccentricity moment.

A complete equivalent static force computer analysis was executed for the structure. More simply for the two storey frame, contraflexure occurs in the bottom column approximately 0.60h from the base, and in the upper storey, approximately 0.65h from the top (1), where h = storey height. A free body diagram of a joint with half columns and beams together with loads which arise in an assumed earthquake is indicated in Fig. 4. The corresponding loading for the joint in the experimental reaction frame is shown in Fig. 5, the main difference being that for the experimental joint, the axial loading in the column acts on line and produces no eccentricity moment on deformation. Hence the loading applied to the joint is a simplified earthquake loading only. The actual loading sequence selected for these tests is shown in Fig. 6 and was adopted from the Hanson and Conner [2] sequence for reinforced concrete joints shown superimposed in Fig.6 although it is considered that for the real structure a lesser ductility of approximately 2 to 2½ would be required. The loads simulate a moderate earthquake followed by a more major earthquake or a preshock followed by the main shock. The adopted loading had two disadvantages.

1. The elastic loading was taken to the yield point (i.e. $\mu = 1.0$), resulting in non-linearities initially.

2. For the second major racking sequence, scanning was from $\mu = +4$ to $\mu = -5$ rather than $\mu = \pm 5$, making the hysteresis loops less stable and it was more difficult to draw a skeleton loading curve.

1.3 EXPERIMENTAL INSTALLATION

The main features of the experimental apparatus can be seen in the photographs appended to this report. Most prominent feature is the reaction frame or test rig. The reaction frame was originally built to test a cruciform joint for the new Bank of New Zealand, Wellington [3].

The column ends were packed between thrust plates using solid steel plates and reaction thrusts were transferred to the 18" reinforced concrete floor of the test hall.

Similar reaction plates and load transfer mechanisms were used for the thrusts on the stub beams. These thrusts were generated by two hydraulic rams (150 US tons capacity and 6 inch stroke), activated by a hydraulic pump. The end of the ram fitted into a circular recess provided, and the loads transferred through a 2" dia. solid rod.

To avoid instability in the plane perpendicular to the test plane, the centre of the joint was bolted to the test hall floor so that on loading rotation took place about that point. Short beams traversed the column ends and were bolted down. These beams were provided to prevent the column from rising in the event of failure. Similar but longer members

traversed the beams but these were not added until testing had extended into a high ductility range and the latter exhibited a tendency to rise and twist slightly at high deflections.

Strain gauges, used to monitor the deformation in the joint, were placed at selected positions and at sites of suspected plastic yielding. Two types of electric strain gauge were used, namely single element gauges and 60 degree three element rosette gauges. The gauges had varying gauge factors but these different gauge factors constituted an error of only -1.9% to + 3.0%.

In total, 68 strain gauges were used, 36 rosettes and 32 straight gauges requiring 140 channels for the output.

The voltage settings on the Wheatstone bridge were such that the voltage output of the strain gauges gave direct strain readings. Output of these 'strain' voltages was fed to a mini data-logger coupled to a teletype output unit. Two forms of output were obtained, viz. a typed output with strain readings next to each gauge number; and a punch tape output for use in association with a 6700 Burroughs Computer.

Axial load in the column was simulated by prestressing with a Macalloy bar (40mm dia.). The required load was 72.32 tons representing 3394 μ-strain based upon a Youngs elastic modulus of 24.5 x 10^6 psi. Two pairs of gauges were used to monitor the prestressing. It was convenient to couple the output of these strain gauges to channels in the data-logger for the main part of the testing. Hence at every scan of the data-logger, an output for the prestressing strains was also given.

The ram pump pressures were monitored from a dial gauge with a capacity of 10,000 psi which could be read to the nearest 100 psi. At 800 psi equivalent to 10 tons ram load the accuracy of loading was ± 1 ton approximately.

Dental plaster was applied to the joint at places of expected yield. It had previously been demonstrated [3] that plaster flaking occurs at yield and that the plaster is a valid indicator for yielding locations.

1.4 PRELIMINARY TESTS AND CALCULATIONS

Tensile tests were carried out on specimens cut from beam flange and column plates at the School of Engineering, University of Auckland. Three specimens were monitored with mechanical extensometers and one using 2 electric resistance strain gauges. The following average results were obtained:

Beam Flanges	σ_y	=	19.35 t/in^2
Column	σ_y	=	20.43 t/in^2
Young's Modulus	E	=	12946 t/in^2

Based upon these figures, applied beam loads to produce first and full plasticity in the star plate were calculated.

In summary,

First yield in star I - section:	33.5 tons
Fully plastic in star I - section:	48.6 tons
First yield in box col. at u/s star:	36.9 tons
First yield in box col. at gauges:	38.4 tons
Fully plastic in box col. at u/s star:	55.4 tons
Fully plastic in box col. at gauges:	57.6 tons

2.1 EXPERIMENTAL PROCEDURE AND OBSERVATIONS

For the purposes of reference to the joint, the following definitions apply. The two columns are called top and bottom columns in the same arrangement as occurs in the real structure, and may be identified with respect to the down hand welding at the beam joints. Beam number 1 is the left hand beam and beam number 2 is the right hand beam in Fig. 1.

An average prestress strain of 3331 μ-strain was obtained at transfer corresponding to 71 tons load. Throughout the testing a loss of prestress was recorded, particularly when the cruciform was loaded. At failure, loss of prestress strain ranged from 499 μ-strain to 613 μ-strain. The rated capacity of the strain gauges by the manufacturers was 2000 μ-strain, after which the voltage strain relationship tends to become non-linear. In addition, during testing, the Macalloy bar was subject to bending, made manifest by the difficulty in removing the prestressing rod after destressing. Thus the extent of real prestressing loss cannot be evaluated and it is suspected not to be as high as the strain readings indicate.

The actual loading pattern to which the cruciform joint was subjected is indicated in Fig. 6. The first two half cycles were mainly in the elastic range up to the theoretical yield load (i.e. 33.5 tons) and loading increased in increments of 6.25 tons, to 31.25 tons. At each incremental increase deflections were plotted and a scan by the data-logger of the gauges was taken. The load was then removed in similar increments and readings taken as before. For the second half cycle it was necessary to reposition the rams on the opposite sides of the stub beams.

On the first half cycle at a jacking load of about 20 tons, some initial plaster flaking took place on beam number 2 at the star plate plastic hinge location. A plot of beam tip deflection versus load, on the reversed elastic half cycle, indicated a deviation from linearity at a deflection of 0.899" and a load of 27.5 tons. This deflection was taken to correspond with a ductility μ of 1.0 and evaluation of higher deflections were based on this.

The following two half cycles were excursions into the plastic range corresponding to ductilities of 2.5 and 5.0. After the ductility = 5.0 half load cycle, extensive plaster cracking was observed in both beams at the plastic hinge locations.

At this stage, shear distortion of the central panels was evident. The singularity of the distortion was unusual.

After high levels of ductility the distortion was quite obvious under an anti-clockwise loading couple (looking down onto the joint), whereas under a clockwise loading couple, rather than an equally opposite distortion developing, the line of the columns and the central panel straightened out.

After the first ductility = 5.0 half cycle, testing was stopped and was resumed again on the following day when the remaining cycling sequences were completed. For the second sequence of elastic cycles, the inbuilt plastic deformations in the joint were considerable and zero load positions of the beam tips were of the order of 0.5" from the original zero load position. This is apparent on studying the hysteresis load-deflection curve.

Following the elastic cycles, three cycles of high ductility followed and very extensive cracking of the plaster occurred. Particularly noticeable was a general shattering of the plaster at the plastic hinge locations, especially on beam No. 2. Plaster cracking extended close to the web centre indicating that a fully developed plastic hinge had been formed as is considered in the theoretical calculations.

At these high levels of ductility, twisting of the beams occurred, the ends tended to lift upwards.

After completion of the predetermined loading pattern, the joint showed no signs of distress and it was decided to create a failure condition and thus observe the failure mechanism of the joint. Loading was therefore increased to produce a ductility = 6.0 and then = 7.0. Increased cracking of the plaster took place, and at this stage yield in the columns was observed together with plaster cracking at weld sites. On the final cycle, aiming for a ductility of 7.0, failure occurred at ductility = 6.54 with a beam load of 55 tons, cracks appeared simultaneously in both star plates at the toes of the column to star plate welds in the areas where the plates are required to resist through thickness tensile stress. These cracks were later found on sectioning and detailed examination to be the visible evidence on the surface of the failure mechanism which began as lamellar tears within the star plates and propogated to the surface under high stress.

The detailed examination suggested that minute lamellar cracks had been present in the star plate prior to the commencement of the loading test but had not been disclosed by the ultrasonic inspection carried out after repairs had been made. A metallographic examination of a section of the failed plate also showed a higher than normal concentration of non-metallic inclusions in the form of manganese sulphides and silicates. These are known to have a very deleterious effect on "through thickness" ductility.

3.1 STRESS HISTORY

Figure 17 shows how the shear stress or principle stress (as indicated) at selected gauge sites varied as the loading proceeded for the first few half cycles. The location of the gauge is indicated in figure 1 by a number system. By inspecting the load history diagrams it can be seen that for the initial load P = 6.25 tons, the stress distribution was low but as the loading proceeded, higher stresses concentrated around the central panel zone, in the starplate, and around the column. These locations were near weld sites and were strongly influenced by weld stress gradients. The theoretical beam jack load for yield in the potential column hinge sites was about 10% higher than for the star plate flange hinges and for the first few load increments stresses at these sites were similar.

For a jack load of 25.0 tons, stresses in the beam flanges and star plate were still low, but stresses in the central panel zone were higher with some yielding locations. For this load, the average shear yield stress, τ_y = 26.4 ksi approximately. Stresses at the potential column hinge site were marginally higher than for the star plate flange hinge site. For the load P = 31.25 tons, there was plastic yielding at six gauge sites and the general level of stress in the panel zone was very high. One point to be noted for all loading cases was that stresses in the vertical central panels of the column were low indicating that the "Poisson's effect" was small. Thus at this location only racking loads did not set up excessive stresses and the two dimensional loading system modelled a three dimensional loading case without excessive error.

For the sequence following, down to zero load, the stresses dropped off to substantially low levels of stress in the joint. At P = 0 tons, some locations of plastic yield persisted, mainly in the central panel zone but also around the star plate and at all the sites where yielding had taken place under the P = 31.25 tons load. Yield stress corresponds to high levels of strain and the gauges may have been over-strained thus throwing suspicion on the reliability of these results. However, as elastic stain readings were reliable anomalous results were attributed to yielding and hence yielding was identified in this way. Because at P = 0 tons yielding sites still existed, then at P = 31.25 tons previously, these sites were considered highly plastic with high levels of ductility, so that the elastic regain on unloading was insufficient to bring the stresses below the plastic level.

As the reversed loading increased, the yielding sites disappeared with a few exceptions, this being consistent with the argument in the above paragraph on yielding sites. During this cycle neither the formation of plastic hinges nor yielding in the star plate occurred at the theoretical design hinge locations as predicted. With a jack load P = 37.5 tons in the third half cycle, the joint made its first excursion into the high ductility range, μ = 2.5, and the central panel zone was well plastic; loading exceeded the theoretical yield load for the star plate flanges (i.e. P = 33.5 tons) but only one yield site existed at the potential hinge location. The elasto-plastic behaviour of the beams was only slight, and similarly for the columns.

With reversed loading, P = 47.5 tons during the fourth half cycle, corresponding to a ductility of 5.0, considerable plastic yielding was evident in the shear panel zone, and reasonably developed elasto-plastic behaviour was evident in the columns. Plastic yielding had also occurred in the star plate flanges and though the elasto-plastic development there was increased, it was still not extensive. It was apparent that most of the yielding had occurred in the central panel shear zone.

The following is a summary of the important points to be noted from the stress investigation.

1. High stress levels and yielding predominantly occur in the central panel zone.

2. Yielding in the star plate flanges occurred as predicted but overall yielding of the joint occurred unpredictably at a lower jack load of P = 27.5 tons.

3. Yielding at the potential column hinge location occurred earlier than expected and at a load less than the yield load for the star plate flanges.

Conclusion number 2 corresponds with a similar conclusion made by Kato [4] ".... due to the existence of residual stress in complicated distribution, exact prediction of the initiation of yielding becomes almost impossible."

3.2 LOAD-DEFLECTION CURVES

The load deflection curves are recorded in figures 8, 9, 10 and 11. In figure 9, attemptshave been made to curve fit the hysteresis curve of Ramberg-Osgood based upon the virgin curve from figure 8.

Considering figure 8, the general turn-over point for the virgin curve is at 27.5 tons load, and 0.899" beam deflection. Deflections plotted are average beam deflections. Deflections plotted are average beam deflections. The curve on return has a bow in it as it passes through zero load, probably due to take up of the column end packing in the reaction frame. It is also evident from the departure of linearity of the first two half cycles, that some elasto-plastic effects were occurring. From consideration of Section 3.1, this elasto-plastic action has been traced to yielding in the central panel shear zone.

The Ramberg-Osgood function may be expressed as (5),

$$\frac{x}{x_y} = \frac{q}{q_y}\left(1 + \left|\frac{q}{q_y}\right|^{r-1}\right)$$

where,

- x = displacement or curvature
- x_y = a characteristic displacement
- q = load or moment
- q_y = a characteristic load
- r = an exponent

x_y, q_y and r are the Ramberg-Osgood parameters, which must be solved simultaneously for a best-fit curve.

A suitable computer programme was developed to find the best-fit curve by least squares method. For the virgin curve shown in figure 8, the following Ramberg-Osgood parameters were found,

- x_y = 1.15 inches
- q_y = 37.5 tons
- r = 9.5

Of interest is consideration of the effects of other chosen parameters on the value of the least squares. For high values of r, for the worst choice of x_y and q_y, least squares errors are of the order 10^{30}, and for small values of r, 10^{15}. Choice of the value of r is more critical than choice of x_y and q_y on the accuracy of the curve fit. The order of magnitude variation of the sum of the least squares is greater for variations in r, than in variations of x_y and q_y.

In generating the hysteresis load deflection curve on reversed loading, Masing's hypothesis may be applied to the Ramberg-Osgood function [6]. This hypothesis states that the hysteretic load-deformation curve can be derived from the virgin curve by enlarging the latter by a factor of two and shifting the origin to the point of last load reversal, i.e.:

$$\frac{x - x_i}{2x_y} = \frac{q - q_i}{2q_y}\left(1 + \left|\frac{q - q_i}{2q_y}\right|^{r-1}\right)$$

where the subscript 'i' refers to the point of last load reversal. Application of Masing's hypothesis in generating the hysteresis curves is shown in figure 12.

Pinkney [6] has reported a similar comparison of hysteresis curves generated by the application of Masing's hypothesis to experimental curves. Pinkney's investigation was for moment-curvature rather than load; in both Pinkney's tests and these tests the results are similar. It can be seen that Masing's hypothesis yields a hysteresis curve similar in shape to that found experimentally, but does not accurately coincide with the experimental curve. The failure of Masing's hypothesis has been overcome by other investigators [7,8] by applying it to the skeleton curve obtained as the locus of points of load reversal for successively larger concentric hysteresis loops - rather than the virgin curve. Additionally, it must be pointed out that accuracy of the virgin curve for ductility levels greater than one ($\mu \geq 1.0$) affects the final predictive power of Masing's hypothesis for reversed cycles. In this analysis the virgin curve was extrapolated and may be in some error in this region.

4.1 BEAM DISPLACEMENTS AND ROTATIONS AND P-$\bar{\gamma}$ CURVE

In order to predict the beam displacements and rotations, a model equivalent to the joint was considered which comprised elements easily dealt with analytically. The beams and columns were treated as one dimensional elements deformable under moment and shear. The central panel zone was

treated as parallel plate elements deformable under shear, and the star plate were allowed to elongate or contract under the action of direct load. Deflections and rotations for the beam were obtained by a semigraphical approach due to the spatial variability of the geometrical moment of inertia.

The results of the investigation are recorded in tables 1 and 2 and the deflections are shown in Fig. 13.

The load deflection curve for the elastic range is reasonably accurately predicted - with approximately 5% under estimate of the experimental results. The calculations indicate that 33.5% of the beam deflection and 46.4% of the joint rotation arise from shear distortion of the central panel. For joint rotations, the rotations of beams with respect to the joint arises from only shear in the beam. Hence, for rotations there are less contributing distortions and shear distortional rotation is a larger percentage of the total rotation than shear distortional deflection is of the total deflection.

Comparing with investigations made by Kato, et al. [9] in association with universal box members, panel shear distortions encountered in this test are relatively large. For the configurations investigated by Kato et al. (namely Universal Box Column sections with either an internal split diaphragm, an external star shaped diaphragm, or a single piece inner diaphragm), panel shear distortion accounted for 17.0% to 22.2% of the beam deflections. This aspect of the star plate joint arrangement together with the early yielding in the panel makes the star plate geometrical confirguration inferior to the configurations investigated by Kato. et al.

The stub beam load P, versus shear distortion (average), $\bar{\gamma}$, curve is well defined for small distortion, from the experimental points, fig. 15. For very large distortions the curve is less certain. This curve may be compared with the predictive equations of Kato [4].

Considering the box shaped column shown in Fig. 14, the shaded area is assumed effective against shear. The couple force F, is

$$F = \frac{M_{b1} + M_{b2}}{h_b} \qquad (1)$$

Average shear $\bar{\tau}$ is,

$$\bar{\tau} = \frac{F}{2h_c t_w} = \frac{M_{b1} + M_{b2}}{2h_b h_c t_w} \leq 0.77\ \sigma_y \qquad (2)$$

Thus, the effective shear volume is,

$$V_p = 2h_b h_c t_w \qquad (3)$$

In the case of a square box column with equal wall thickness,

$$V_p = \frac{1}{2} V \qquad (4)$$

where: V = total volume of connection part surrounded by beam and column ends

If ℓ = length of stub beam lever arm to moment face M_{b1} or M_{b2} and

P = jack load,

then the P - $\bar{\gamma}$ predictive equation becomes

$$\tau = \frac{P \times \ell + P \times \ell}{2\ h_b h_c t_w} \qquad (5)$$

but as $\bar{\gamma} = \tau / G$

where $\bar{\gamma}$ = average shear distortion

$$\text{then,} \quad \bar{\gamma} = \frac{P\ell}{G} \left(\frac{1}{h_b h_c t_w}\right) \qquad (6)$$

For Design purposes, the limiting case becomes,

$$\bar{\gamma} \leq \frac{0.77\sigma_y}{G} \qquad (7)$$

The experimental P - $\bar{\gamma}$ curve is plotted in Fig. 15, and the predictive P - $\bar{\gamma}$ curve is also plotted (dotted line). The limiting Jack load for elastic shear panel distortion is also indicated at P = 42.55 tons. Kato's equation predicts a slightly more flexible shear region. This difference from the experimental curve is readily accounted for by the fact that gauge sites are near welds and heavy stiffeners, e.g., the star plate. Distortions are measured near the edge of the plate and will be less than at the centre. The average shear distortion thus evaluated is lower, resulting in an apparently stiffer plate.

The experimentally obtained average shear distortion $\bar{\gamma}$ was obtained from six gauge sites.

The general yield point as determined by non-linearity in the load deflection curve, is well into the non-linear range of the P - $\bar{\gamma}$ curve.

Equation (6) (Kato) grossly overestimates the actual shear yield point in the joint and this result from the use of Kato's equation suggests that the joint performed unsatisfactorily. The geometry of the star plate joint is somewhat more complex (in that the star plate is continuous through the column), than that shown in Fig. 14; the possibility must not be overlooked that Kato's equation - based on a simple geometry joint - maybe unsatisfactory for prediction with a more complex geometry joint. An unusually high proportion of the load is absorbed in the shear panel resulting in early non-linearities in the star plate cruciform joint.

The approach used for the joint analysis by Kato is similar to that given by Fielding and Chen [13], i.e., by consideration of the average yield stress distributed over the shear panel. The shear stress is given by Fielding and Chen as,

$$\bar{\tau} = \frac{1}{d_c t_p} \left(\frac{M_r}{d_g} + \frac{M_\ell}{d_g} - \frac{V_a}{2} - \frac{V_b}{2}\right) \qquad (8)$$

Where M_r & M_ℓ = bending moments acting on the right and left sides of a connection.

V_a & V_b = the individual column shears above and below the connection

d_g = the girder depth

d_c = the column depth

t_p = the column web thickness.

This may be rearranged to,

$$\bar{\tau} + \frac{1}{d_c t_p}\left(\frac{V_a}{2} + \frac{V_b}{2}\right) = \frac{1}{d_c t_p}\left(\frac{M_r}{d_g} + \frac{M_t}{d_g}\right) \qquad (9)$$

The terms V_a and V_b are not included in the equations developed by Kato, but their effect cannot be ignored. Kato allows for the effect by putting $\frac{4}{3}\bar{\tau}$ for the shear stress in equation 9. This implies that the terms $\{V_a, V_b\}$ contributes 33% to the shear deformation. By evaluating Fielding and Chens equations for the joint, the terms $\{V_a, V_b\}$ actually contribute 18.6% to the shear deformation. Thus Kato's equation overestimates the yield deformation load for this joint as shown in Fig. 15.

The effect of axial force on the yield response of a beam-to-column joint was investigated by Fielding and Huang [14]. Their interaction equation based on the Von Mises yield criterion gives,

$$t_p > \frac{\sqrt{3}\left(\frac{M_r}{d_g} + \frac{M_\ell}{d_g} - \frac{V_a}{2} - \frac{V_b}{2}\right)}{\sigma_y d_c \sqrt{1 - \left(\frac{P_c}{P_y}\right)^2}} \qquad (10)$$

where P_c = column axial load.

P_y = column axial yield load.

This relationship reduces to equation (8) when the axial load is small as the term under the square root then approximates unity; equation (10) gives no insight into the premature yielding of the central panel zone.

Sherbourne [15] reported an analytical study of steel beam-to-column joints where the column was idealised as a plate in plain stress loaded by in-plane forces from the connecting beams. Of several approaches available he found the finite element method most satisfactory. As a result of using such an analytical method in the analysis of a large number of external and internal beam-to-column joints, Sherbourne proposed a number of design equations. The equations relevant to the joint reported here are,

$$\alpha_c = 1.00 - 0.50\,(P_c/P_y) - 0.50\,(P_c/P_y)^2 \qquad (11)$$

$$P_w = \sigma_y t_p\,(t_f + 6\,k_c)\,\alpha_c \qquad (12)$$

where P_w = ultimate beam flange force that may be carried by an unstiffened web.

t_p = thickness of column web

t_f = thickness of beam flange

k_c = column ' K ' distance (sic)

The leading values are; P_c = 71 tons, P_y = 812 tons, σ_y = 20.43 t/in^2, t_p = 2x0.75 = 1.5", t_f = 0.625", k_c = 0.75" (no fillet) and the equations yield,

α_c = 0.96; Pw = 150.7 tons.

This corresponds to a beam jack load of P = 39.1 tons.

Sherbourne has treated interior and exterior connections separately because the mode of failure was different in each case. Sherbourne found that web failure in interior connections was primarily due to the large normal stresses opposite the beam flanges, in exterior connections it was due to the high shear stresses induced in the web by asymmetrical beam loading. Consideration of the loading assumed by Sherbourne for interior connections indicates symmetrical loading and no high asymmetrical shear loading. Thus the expressions given by Sherbourne for the exterior connections better reflect the state of stress in the joint reported here.

viz $$P_w = \frac{1}{2}\left(\frac{\sigma_y}{\sqrt{3}}\, t_p d_c \alpha_c\right) \qquad (13)$$

where d_c = depth of column (14").

The coeffeicient, 1/2, arises from the fact that Sherbourne considered only one beam abutting the column (viz external joint). Substituting in the leading values, then

α_c = 0.96, Pw = 119.0 tons

This corresponds to a beam jack load of P = 30.8 tons. The general yield was observed at 27.5 tons. Thus "premature" yield in the central panel zone has been reasonably closely predicted by using an expression developed for exterior joints but applied here because of the implicit assumption of high shear stresses in the web.

Fielding and Chen [13] give theoretical expressions for the elastic and plastic slopes of the P - $\bar{\gamma}$ diagram with the results also shown in Fig. 15. It can be seen that the plastic slope is very flat. Shear stress can not in practice be uniform over the shear panel, the edges remaining elastic or elasto-plastic until the flanges of the adjoining beam become completely plastic. This gives rise to the plastic slope - neglecting strain hardening. Thus a flat slope indicates an extensive distribution of plasticity over the shear plate, and a lower level of plastic shear resistance can be expected.

The ultimate strength of a member is not affected by residual stresses or inbuilt stresses (10,11), except in stability problems (12) - unless the geometry is considerably changed by the deformations. The ultimate strength stub load for this star plate joint was 55 tons. The theoretical fully plastic load for the star I section was 48.6 tons. Hence,the ultimate strength of the joint is not lowered, and from a structural point of view the joint has peformed satisfactorily in the ultimate

strength range.

4.2 DUCTILITY RATIOS

The ductility factor, denoted by μ, is a variously defined parameter, but is generally recognised as being the ratio of total deformation to elastic deformation at yield. Expressed in terms of deflection, then the ductility factor can be interpreted as being in terms of the imemdiately preceding zero load configuration or in terms of an initial zero configuration. The latter definition was used in the star plate experiments.

Plasticity ratio, denoted by π_d, is exactly defined for deflections as the ratio of residual plastic deformation Δ' to elastic deformation at yield Δ. Popov and Pinkney consider this to be a better dimensionless parameter for plastic deformations.

4.3 CYCLIC ENERGY DISSIPATION

The energy dissipated by one ½ - cycle is represented by the area under the load - deflection curve. Cyclic energy dissipation is related to displacements, and it is convenient to investigate a relationship, e versus π_d , where,

$$e = W/(\tfrac{1}{2}\Delta_p P_p)$$

where W = energy dissipation for one-half cycle.

The parameters P_p and Δ_p in this context are not clearly defined by Popov and Pinkney [7] when using the relationship; however here it has been interpreted as the yield load and deflection. The results from Popov et al. investigation are given in Fig. 16 with the results from these investigations superimposed. The results lie above the average found by Popov et al, but similarly, the low values of π_d, the points are well clustered around a best fit line.

Popov and Pinkney propose that the line, $e = 1.77\ \pi_d$ is a reasonable estimate for relating energy absorption to plastic displacement for at least two types of steel tested. There may, however, be a shift in the line for substantial changes in the geometry of the joint. It is important to point out the curved part of the hysteresis curves, from which the energy dissipation has been evaluated, has been estimated only, to pass through the experimental points. The authors consider the curves, however, reasonable estimates of the probable response - they follow the general curve predicted by the Ramberg-Osgood function.

4.4 TOTAL ENERGY DISSIPATION

Failure points may be expressed in terms of accumulated energy ratio Σe, versus accumulated plasticity ratio, $\Sigma\pi_d$, where the summation is carried over the total number of excursions for the test. The results are given in Fig. 17, in comparison with failure points for joints investigated by Popov and Pinkney [7]. Interpretation, however, is mainly qualitative and again the effects of variations in joint geometry and non-uniform load cycling is not clear.

5.1 CONCLUSIONS

Because only one test was carried out on this type of joint, definite conclusions can not necessarily be drawn on star plate cruciform joint yield response in general. However, the following conclusions may be reached for the joint tested,

1. The general yield point is unpredictable and the distribution of stress throughout the joint for the location of initial yield is not obvious.

2. The central panel shear zone is a critical feature of the joint and governs a high percentage of the overall yield response of the joint.

3. Predictive theories on the joint response given by Kato and Feilding and Chen over-estimate the turn over point of the P- $\bar{\gamma}$ diagram, more so for Kato's theory than for Fielding et al. An assumption made by Kato in respect to the amount of shear distortion caused by column shear is excessive for this joint layout, resulting in the larger error.

Application of data fitted design formulae based on finite element studies of a large number of joints, developed by Sherbourne, may be used to predict yield in the central panel zone provided note is taken of the nature of the yield failure implicitly assumed in the formula.

4. Masing's hypothesis applied to the Ramberg-Osgood function results in load-deflection hysteresis curves of the correct shape, but prediction of the exact curve is not good. The Ramberg Osgood function was applied to the virgin load-deflection curve. Pinkney suggests application of the Ramberg-Osgood function to the skeleton curve would result in a better line.

5. The type of loading history used for this test and the manifestly complex response of these joints to that loading was not entirely satisfactory for the analytical treatment of the results conducted later; component responses are more readily identified with a simpler loading regime. Simulated earthquake loading results in unstabilised hysteresis curves. Uniform loading or gradually increasing loads on the beams would have been more satisfactory as the skeleton load deflection curve can be then found.

6. The ultimate strength of the joint was higher than theoretically estimated, but as shown by the test and as confirmed by more recent theoretical studies, most of the elastoplastic yielding takes place in the central panel zone. A repeat design of star plate type joints would need to recognise this fact and the panel zone proportioned accordingly.

7. Cyclic energy dissipation and total energy dissipation, though not readily useful from a design point of view, are a useful basis for an appraisal of joint response and for comparison of different

types of joints. In this test uniform post elastic load cycling would have given a better comparison with other joint types.

8. In the close vicinity of the welds theoretical joint stresses tend to be masked by in-built stresses due to welding during fabrication. Thermal strains due to weld shrinkage under high restraint conditions can impose near yield or yield stresses in the adjacent metal and these may affect the performance of the joint. Of considerable importance in star plate type joints is the through thickness stresses set up by welding. Exact stress levels are unknown and cannot be determined by the test.

6.1 ACKNOWLEDGEMENTS

The authors wish to extend their thanks to the Commissioner of Works for permission to publish this paper and to Professor N. A. Mowbray for offering the use of the reaction frame and the facilities at the Engineering School, University of Auckland.

REFERENCES

1. Sutherland, H. and Bowman, H. L., "Structural Theory", 3rd Edn, John Wiley and Sons, New York, 1944.
2. Hanson, N. W. and Conner, H. W., "Seismic Resistance of Reinforced Concrete Beam Column Joints", Proc. ASCE, Vol. 93, No ST5, October, 1967, pp 533-560.
3. Shepherd, R. and Spring, K. C., "Racking Load Tests on a Steel Beam Column Joint", - to be published in New Zealand Engineering.
4. Kato, B., "A Design Criteria of Beam-to-Column Joint Panels", Bulletin of the New Zealand National Society for Earthquake Engineering, Vol. 7, No. 1, March, 1974.
5. Kaldjian, Mouses J., "Moment - Curvature of Beams as Ramberg-Osgood Functions", Proc. ASCE, Vol. 93, No ST5, October, 1967, pp 53-65.
6. Pinkney, R. B., "Cyclic Plastic Analysis of Structural Steel Joints", Report No. EERC 73-15, University of California, Berkley, August 1973.
7. Popov, E. P. and Pinkney, R.B., "Cyclic Yield Reversal in Steel Building Connections", Proc. ASCE, Vol. 95, No. ST3, March, 1969.
8. Morrow, Jo Dean, "Cyclic Plastic Strain Energy and Fatigue of Metals", Internal Friction, Damping and Cyclic Plasticity, STP-378, ASTM, 1965, pp 45-84.
9. Kato, B., Fijita, F. and Okano, K. "Manufacture and Structural Characteristics of Universal Box Members", to be published in the Bulletin of the New Zealand National Society for Earthquake Engineering.
10. Baker, J. F., Horne, M. R. and Heyman, J., "The Steel Skeleton", Cambridge University Press, 1956, Vol. 2.
11. Jez-Gala, Carmen, "Residual Stresses in Rolled I-sections", Proc. Instn Civ. Engrs., Vol. 23, November 1962, p. 361.
12. Massonett, C. E. and Save, M. A., "Plastic Analysis and Design" - Blainsdell Publishing Company, New York 1965.
13. Fielding, D. J. and Chen, W. F., "Steel Frame Analysis and Connection Shear Deformation", Proc. ASCE, Vol. 99, No ST1, January 1973, pp 1-18.
14. Fielding, D. L. and Huang, J. S., "Shear in Steel Beam-to-Column Connections", Supplement to the Welding Journal, July 1971, pp 313s - 326s.
15. Sherbourne, A. N., "New Developments in Steel Beam-to-Column Connections".

TABLE 1

Jack Load (tons)	δ_{bc} (inches)	δ_{bs} (inches)	$\delta_{bd} + \delta_{bb}$ (inches)	δ_{τ} (inches)	δ_{actual} (inches)
6.25	0.0407	0.0725	0.0652	0.1784	0.2055
12.5	0.0814	0.1451	0.1304	0.3569	0.386
18.75	0.1221	0.2176	0.1955	0.5353	0.55
25.0	0.1628	0.2901	0.2607	0.7136	0.7635
31.25	0.2035	0.3626	0.3259	0.8920	1.123

TABLE 2

Jack Load (tons)	ϵ_{bc} (radians)	ϵ_{bs} (radians)	ϵ_{bb} (radians)	θ_{t} (radians)
6.25	0.000463	0.000894	0.000138	0.001495
12.5	0.000926	0.001788	0.000276	0.002990
18.75	0.001388	0.002681	0.000413	0.004482
25.0	0.001850	0.003575	0.000550	0.005975
31.25	0.002313	0.004469	0.000688	0.007470

All deflections are in inches and all rotations are in radians.

δ_{bc} = deflection beam due column

δ_{bs} = deflection beam due shear panel

δ_{bd} = deflection beam due diaphragm (Star Plate)

δ_{bb} = deflection beam due beam

δ_{bc} = rotation beam due column

ϵ_{bs} = rotation beam due shear panel

θ_{bb} = rotation beam due beam

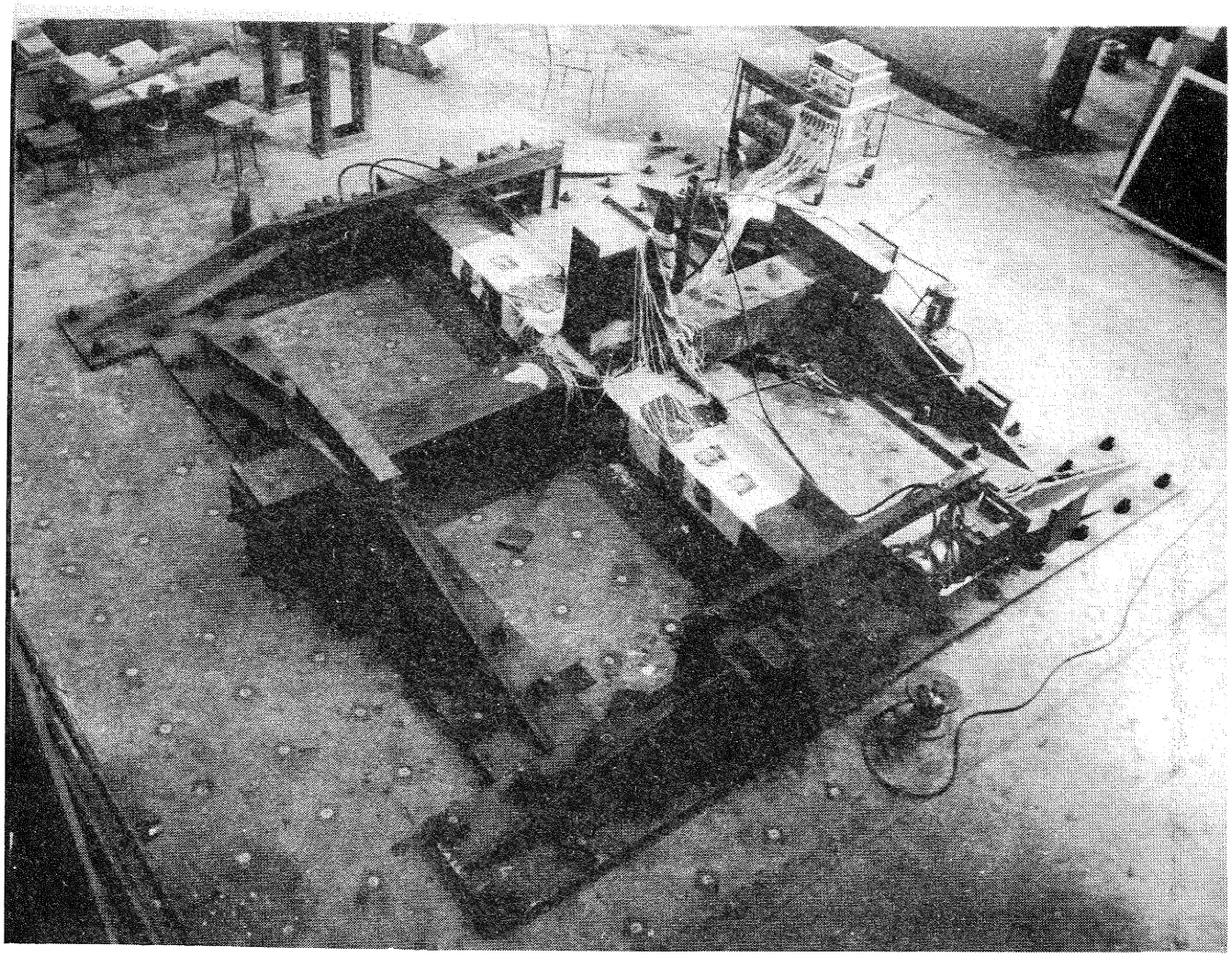

GENERAL VIEW OF TEST IN PROGRESS

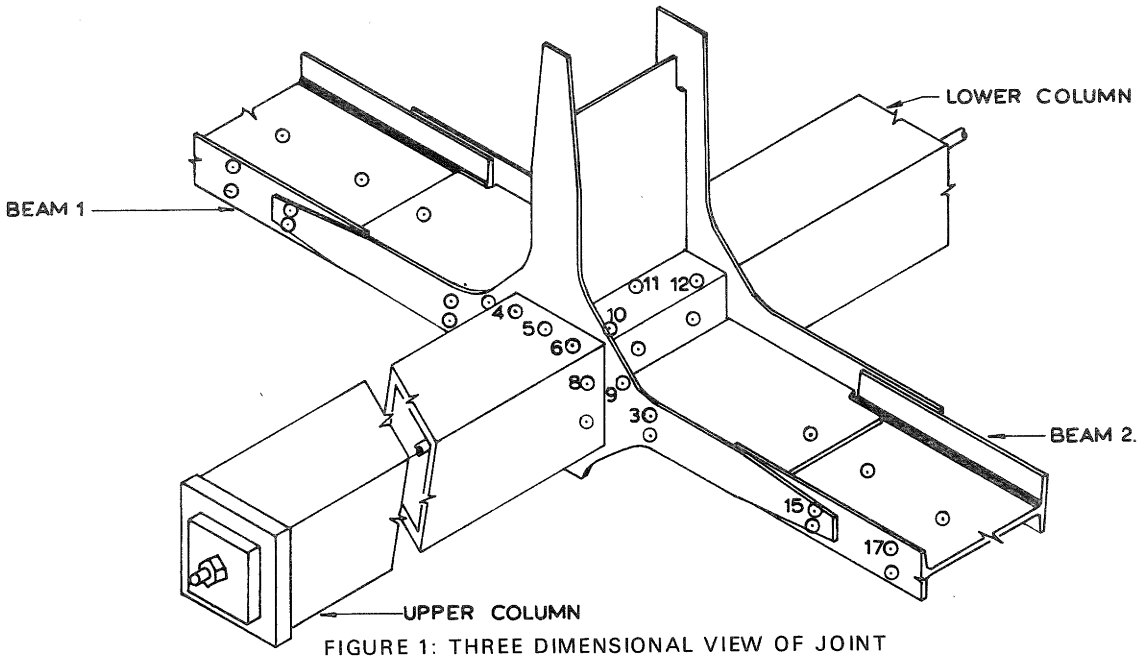

FIGURE 1: THREE DIMENSIONAL VIEW OF JOINT

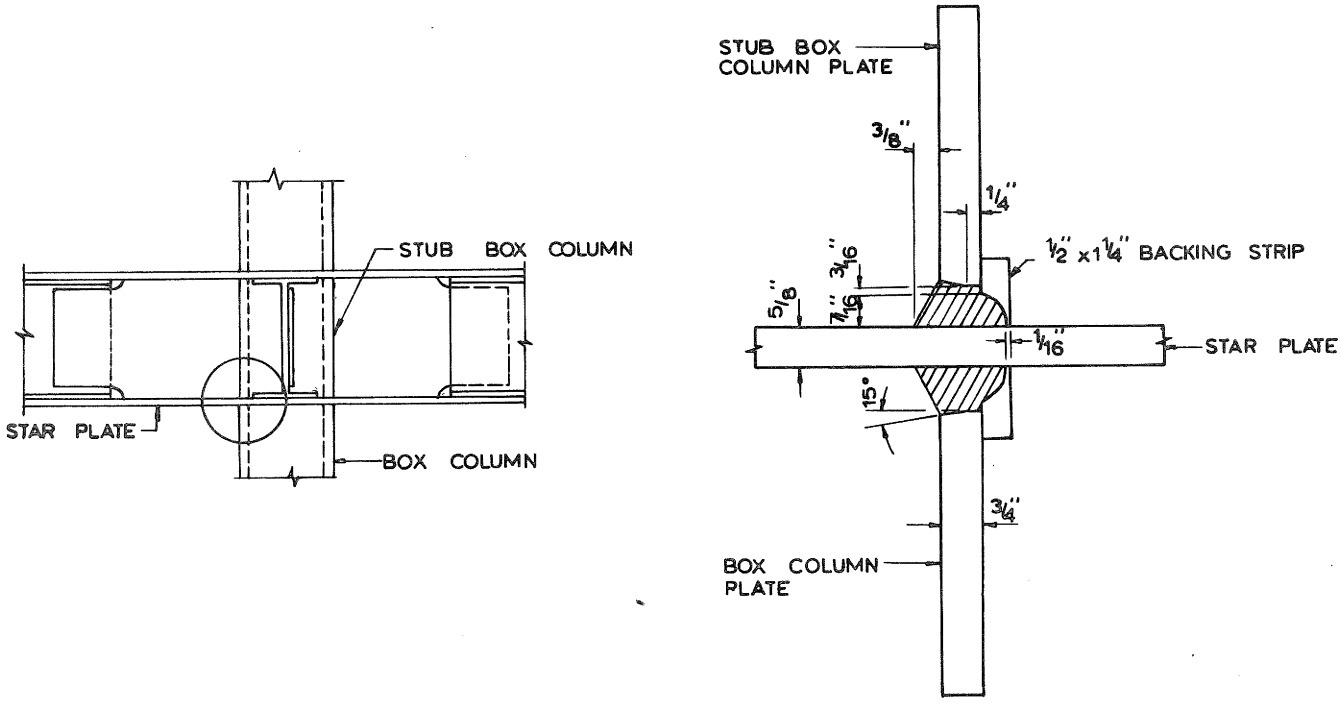

FIGURE 2: DETAIL OF COLUMN TO STAR PLATE BUTT WELD

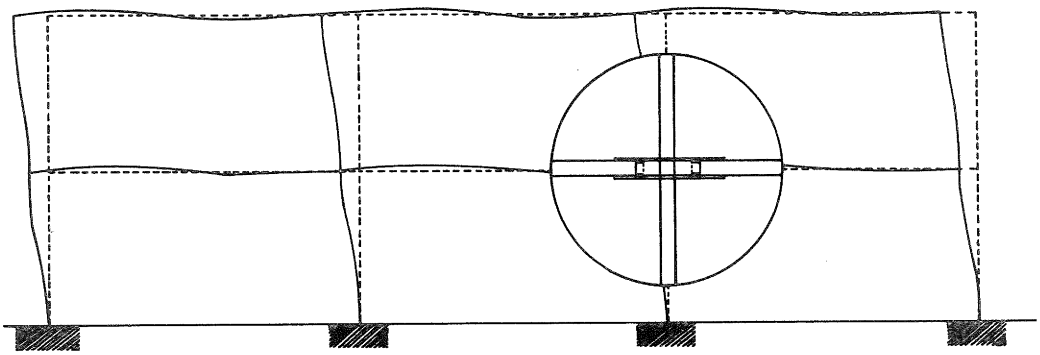

FIGURE 3: SECTION THROUGH BUILDING FRAME

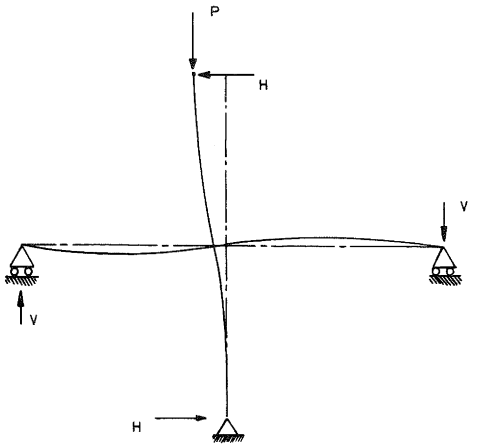

FIGURE 4: FREE BODY DIAGRAM OF JOINT

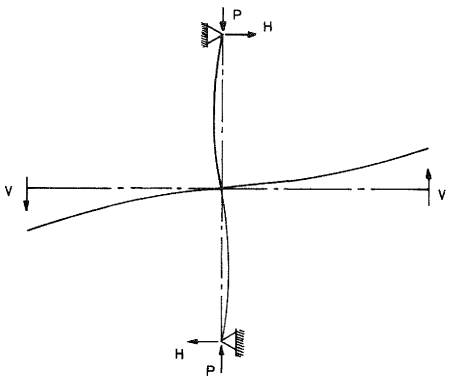

FIGURE 5: LOADING IN THE REACTION FRAME

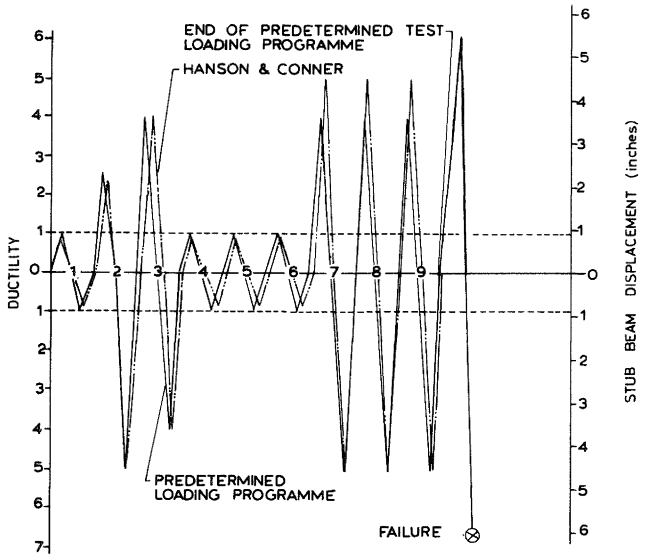

FIGURE 6: THE LOADING SEQUENCE

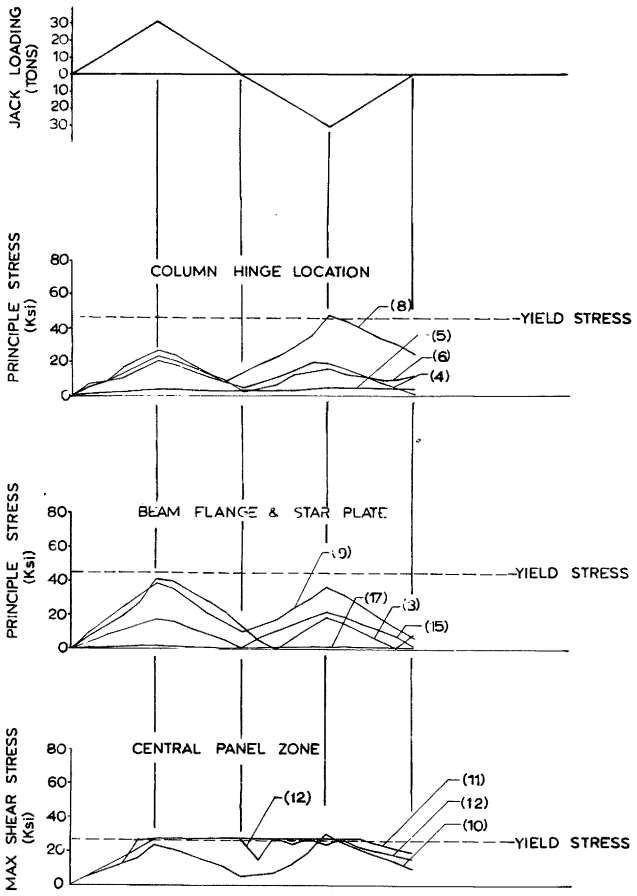

FIGURE 7: STRESS HISTORY AT SELECTED GAUGE SITES

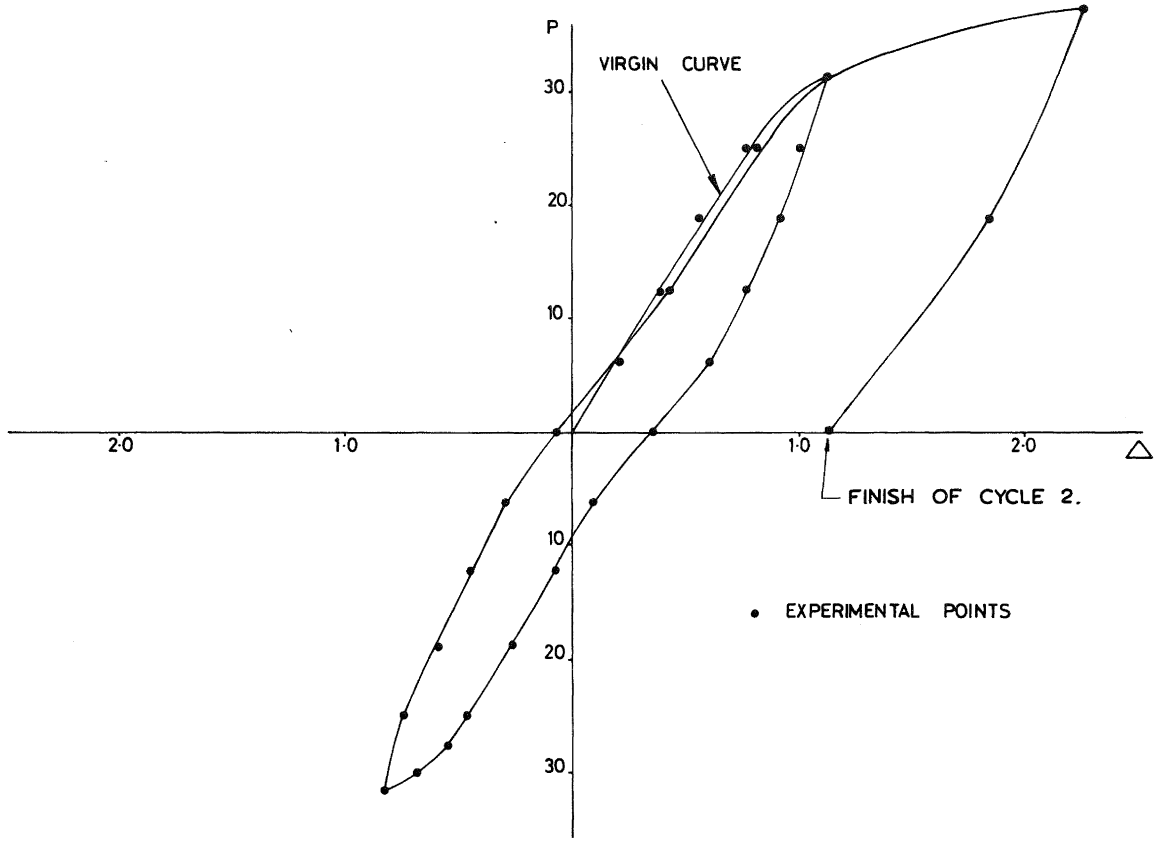

FIGURE 8: LOAD DEFLECTION HYSTERESIS CURVE (1)

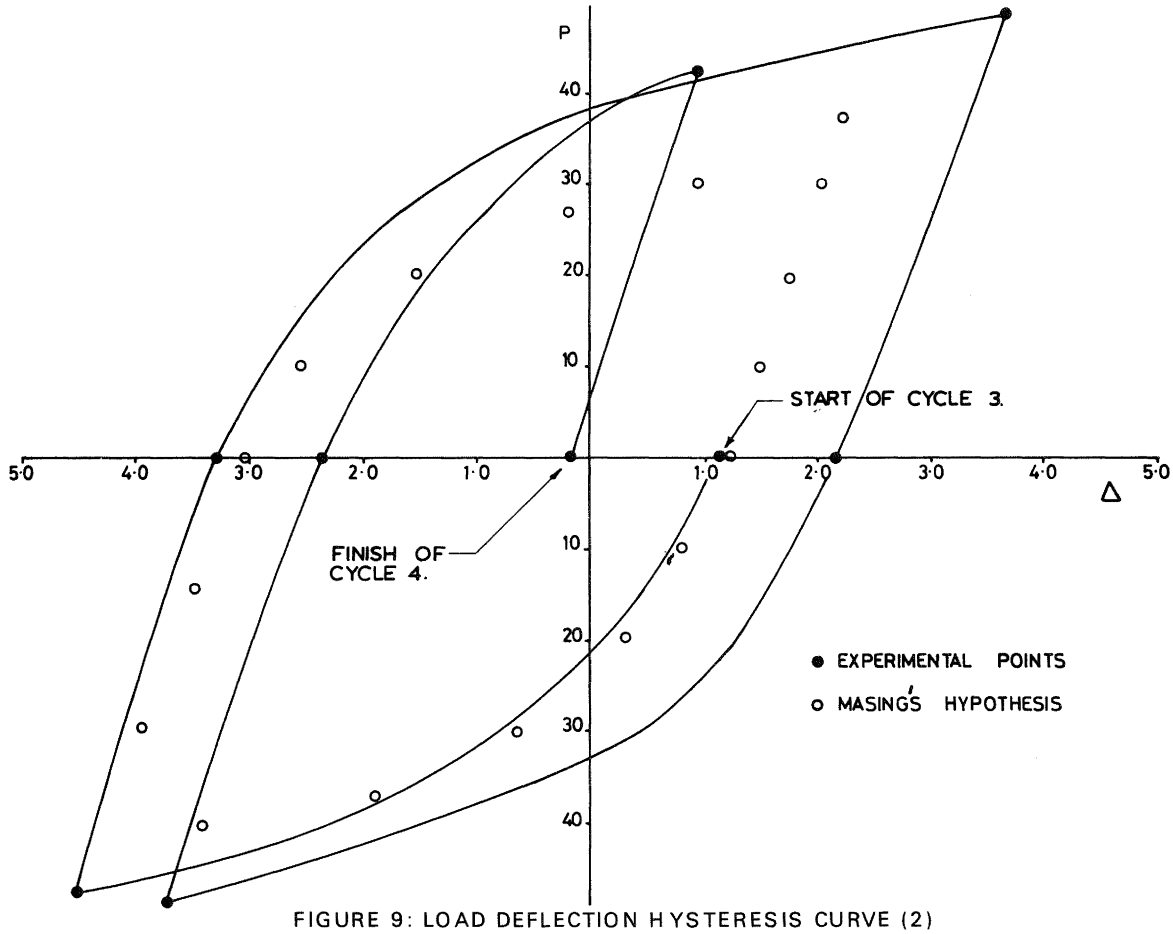

FIGURE 9: LOAD DEFLECTION HYSTERESIS CURVE (2)

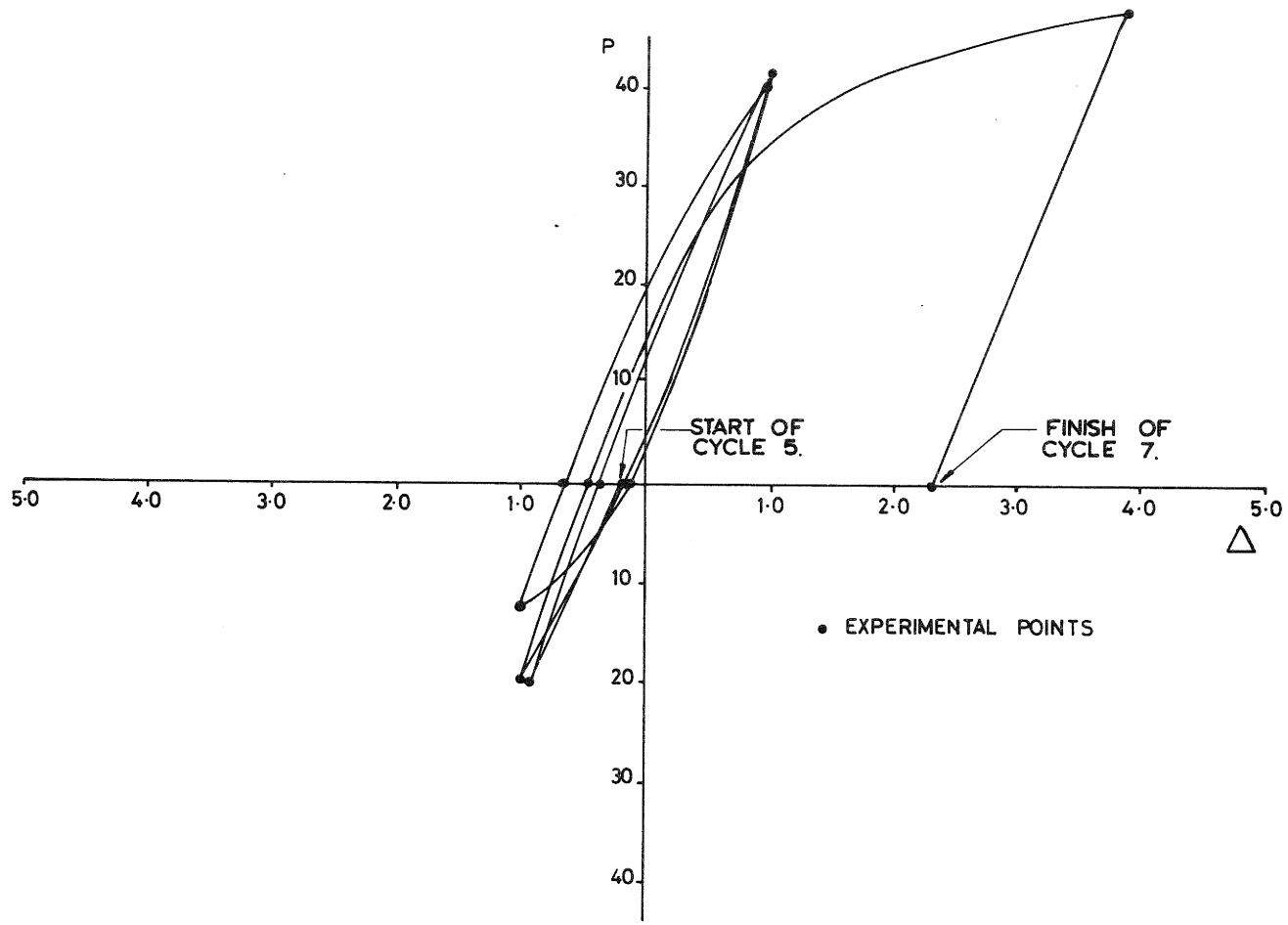

FIGURE 10: LOAD DEFLECTION HYSTERESIS CURVE (3)

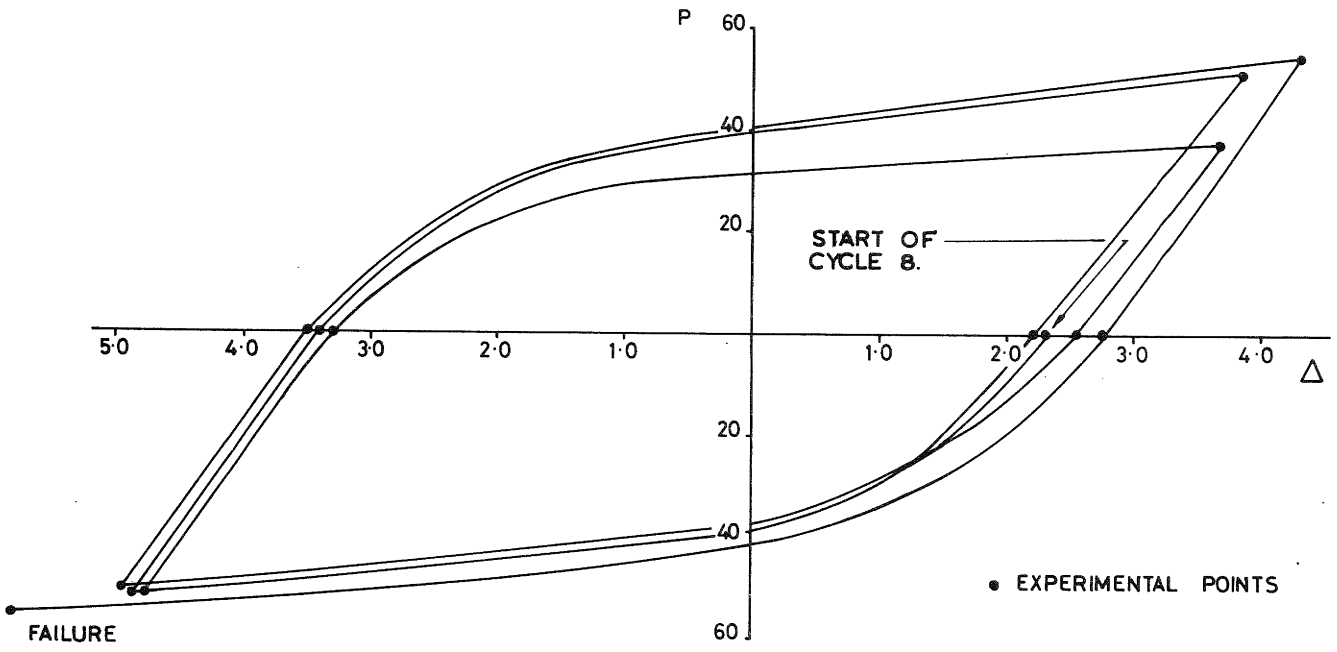

FIGURE 11: LOAD DEFLECTION HYSTERESIS CURVE (4)

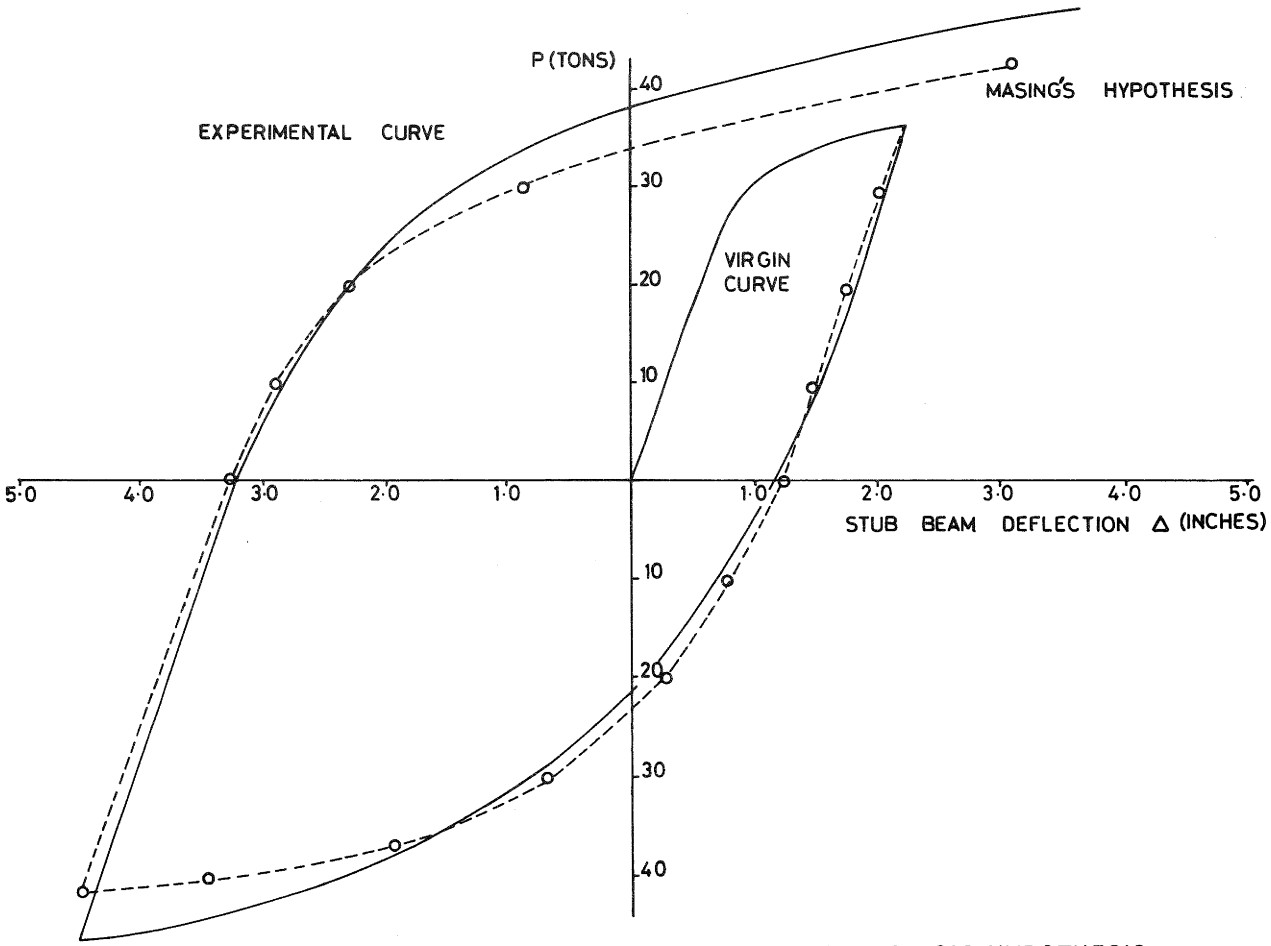

FIGURE 12: EXPERIMENTAL HYSTERESIS CURVE VERSUS MASING'S HYPOTHESIS

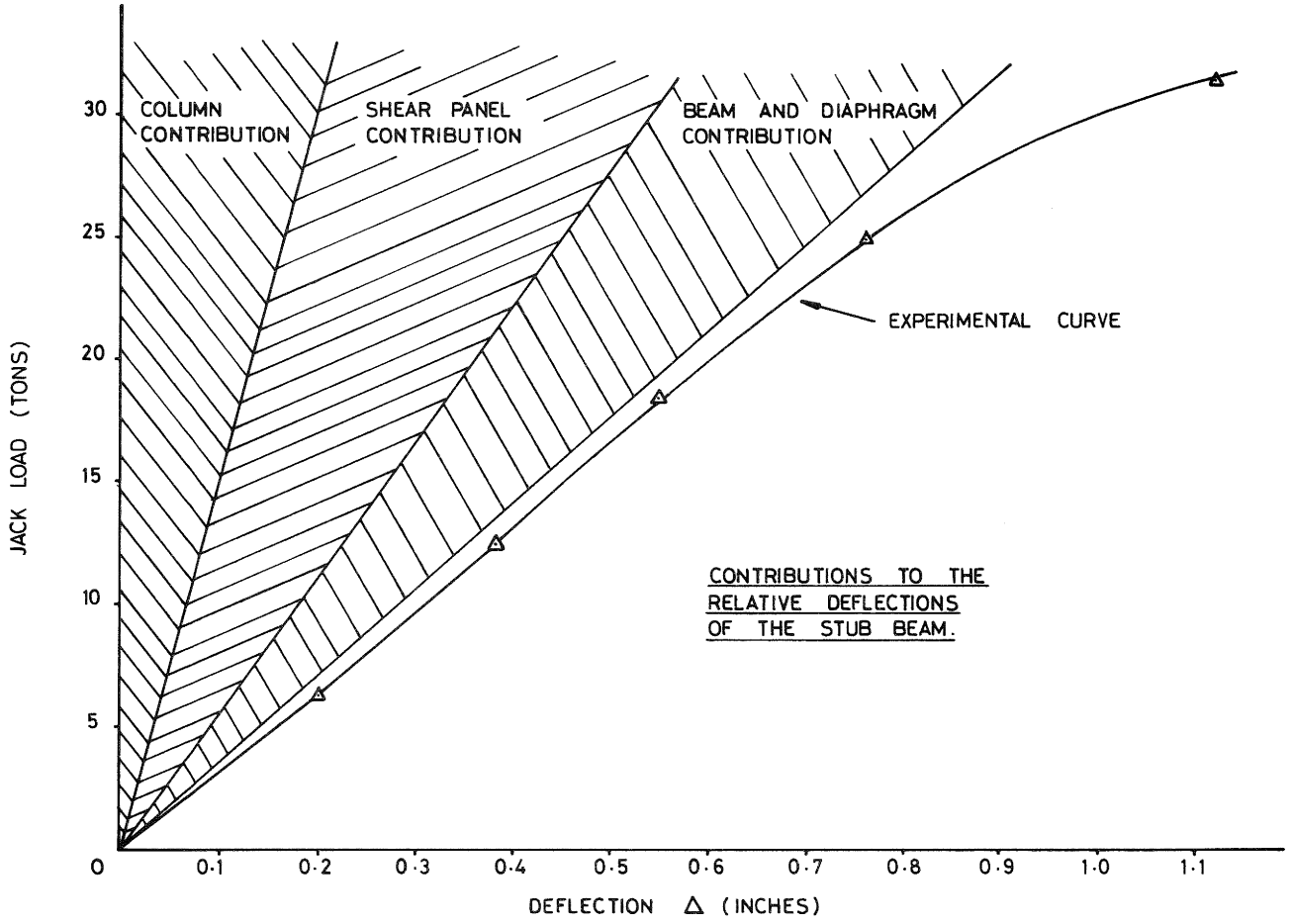

FIGURE 13: STUB BEAM DEFLECTIONS

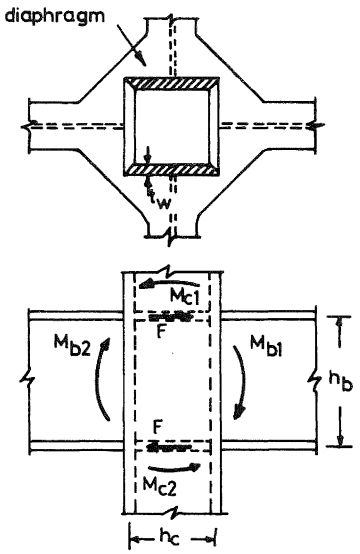

FIGURE 14: BOX SHAPED COLUMN JOINT (AFTERKATO)

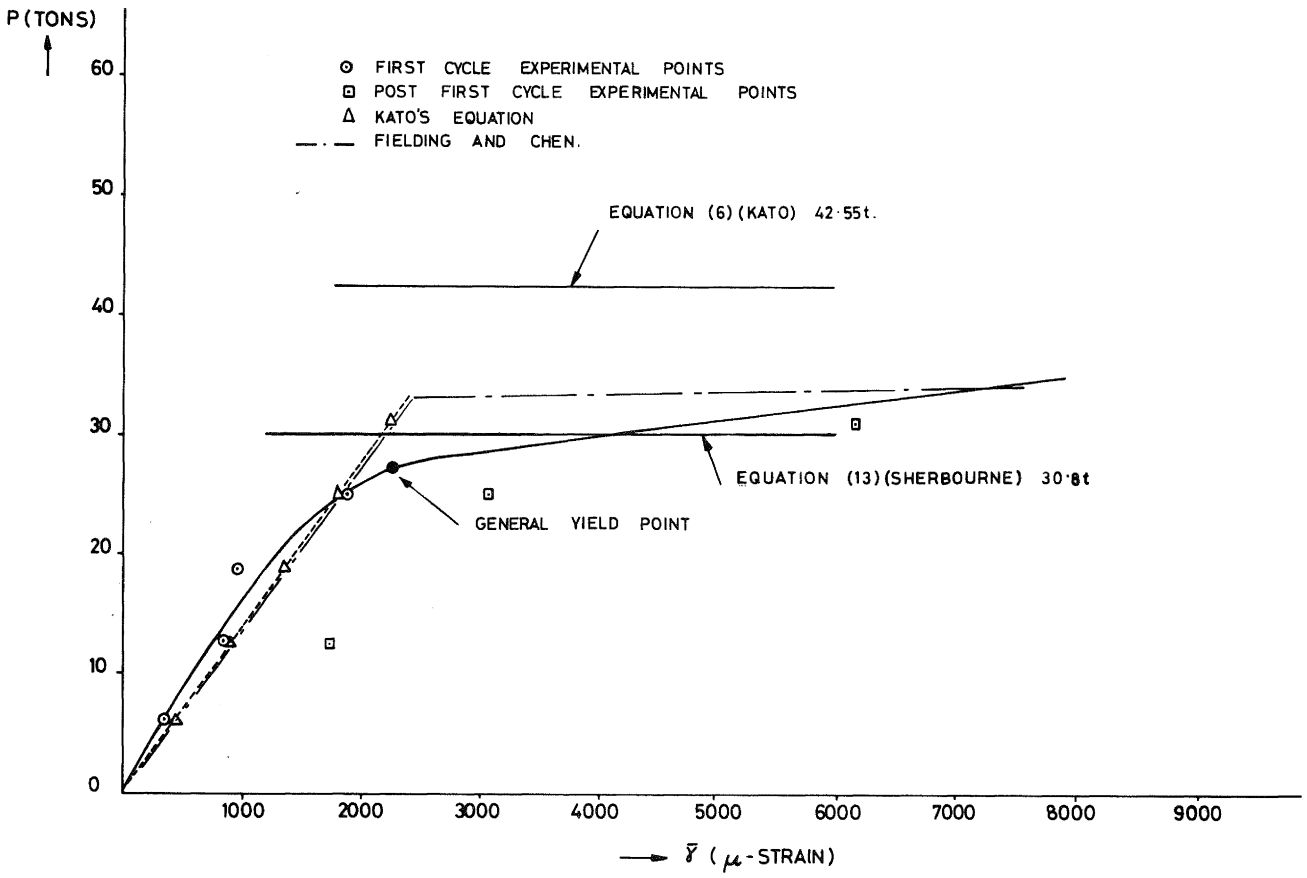

FIGURE 15: THE P - $\bar{\gamma}$ CURVES

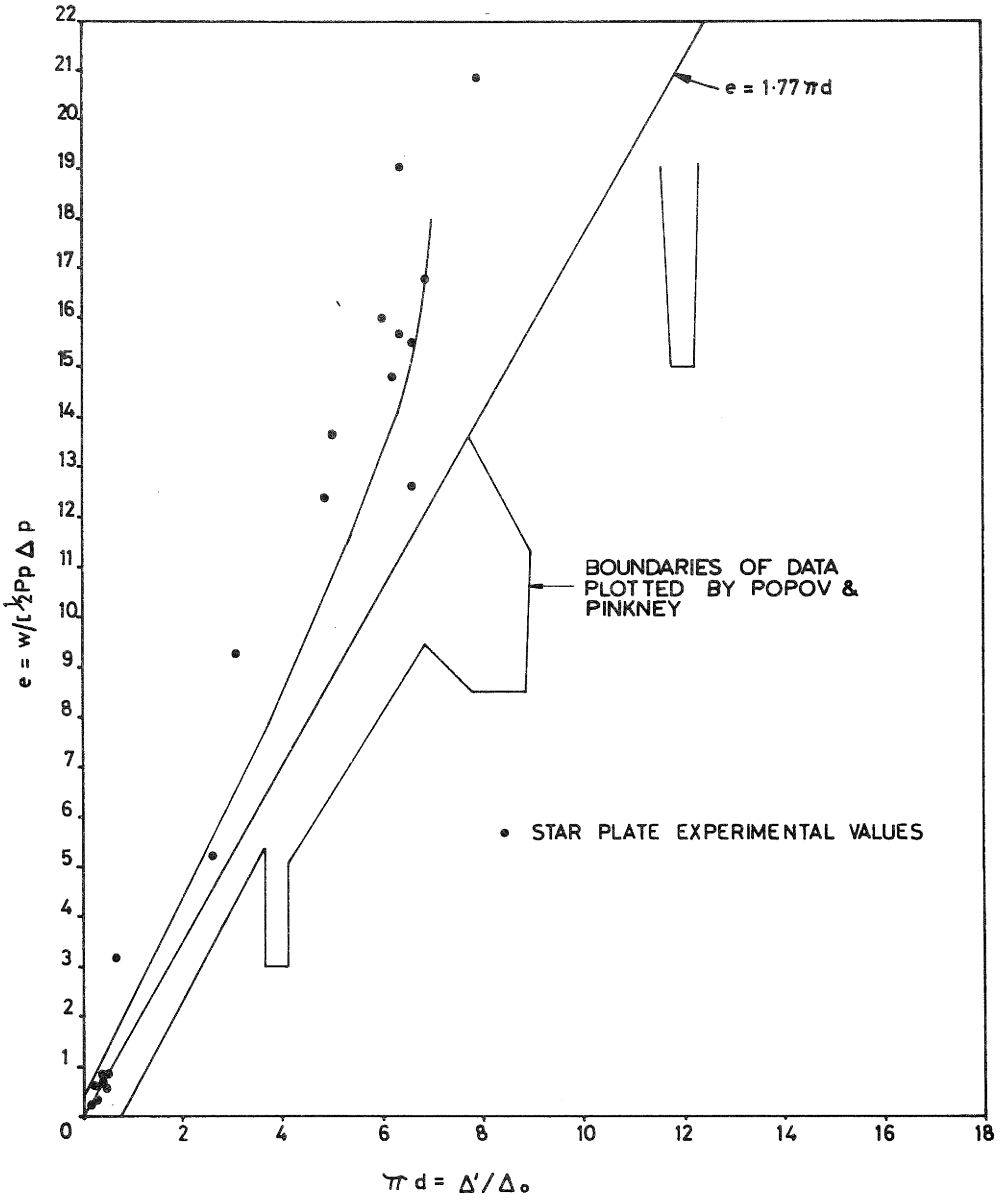

FIGURE 16: ENERGY RATIO VERSUS PLASTICITY RATIO. (AFTER POPOV & PINKNEY)

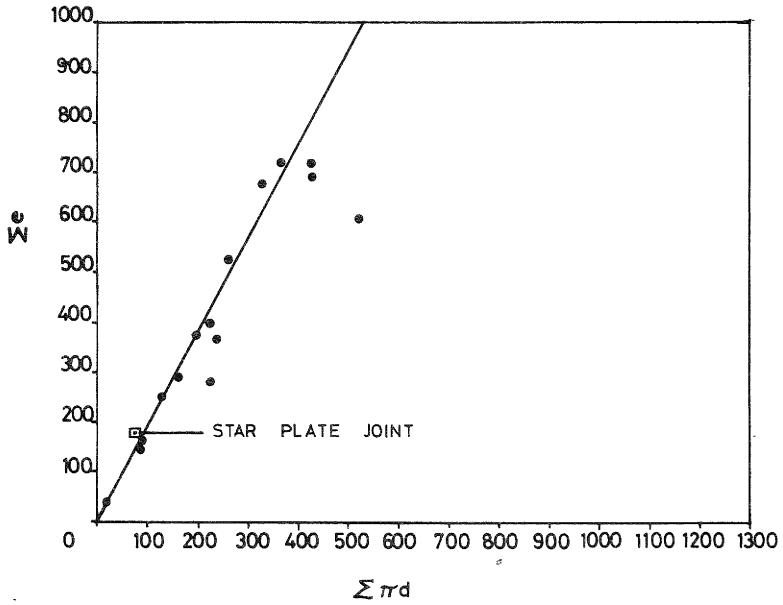

FIGURE 17: ACCUMULATED ENERGY RATIO VERSUS ACCUMULATED PLASTICITY RATIO (AFTER POPOV & PINKNEY)